Neurobiology of Disease

Different Intracellular Pathomechanisms Produce Diverse *Myelin Protein Zero* Neuropathies in Transgenic Mice

Lawrence Wrabetz,[1]* Maurizio D'Antonio,[1]* Maria Pennuto,[1] Gabriele Dati,[1] Elisa Tinelli,[1] Pietro Fratta,[1] Stefano Previtali,[2] Daniele Imperiale,[1] Jurgen Zielasek,[3] Klaus Toyka,[3] Robin L. Avila,[4] Daniel A. Kirschner,[4] Albee Messing,[5] M. Laura Feltri,[1] and Angelo Quattrini[2]

[1]DIBIT and [2]Department of Neurology, San Raffaele Scientific Institute, 20132 Milano, Italy, [3]Department of Neurology, University of Würzburg, D97080 Würzburg, Germany, [4]Biology Department, Boston College, Chestnut Hill, Massachusetts 02467, and [5]Waisman Center and Department of Pathobiological Sciences, School of Veterinary Medicine, University of Wisconsin, Madison, Wisconsin 53706

Missense mutations in 22 genes account for one-quarter of Charcot–Marie–Tooth (CMT) hereditary neuropathies. *Myelin Protein Zero* (*MPZ*, *P0*) mutations produce phenotypes ranging from adult demyelinating (CMT1B) to early onset [Déjérine-Sottas syndrome (DSS) or congenital hypomyelination] to predominantly axonal neuropathy, suggesting gain of function mechanisms. To test this directly, we produced mice in which either the *Mpz*S63C (DSS) or *Mpz*S63del (CMT1B) transgene was inserted randomly, so that the endogenous *Mpz* alleles could compensate for any loss of mutant P0 function. We show that either mutant allele produces demyelinating neuropathy that mimics the corresponding human disease. However, P0S63C creates a packing defect in the myelin sheath, whereas P0S63del does not arrive to the myelin sheath and is instead retained in the endoplasmic reticulum, where it elicits an unfolded protein response (UPR). This is the first evidence for UPR in association with neuropathy and provides a model to determine whether and how mutant proteins can provoke demyelination from outside of myelin.

Key words: **Charcot–Marie–Tooth neuropathy; myelin protein zero; packing; Schwann cell; traffic; transgene**

Introduction

Charcot–Marie–Tooth (CMT) neuropathies are characterized by progressive distal weakness and muscle atrophy, foot deformities, impaired tendon reflexes, and usually minor sensory symptoms (Suter and Scherer, 2003; Wrabetz et al., 2004a). Nerve conduction velocities (NCVs; <38 m/s) and morphology distinguish demyelinating from axonal subtypes. Duplication of a segment containing *peripheral myelin protein 22 kDa* (*PMP22*) within chromosome 17 accounts for about one-half of CMT neuropathies, but point mutations in 22 genes account for another one-fourth. Dominantly inherited mutations in *myelin protein zero* (*MPZ*, *P0*) cause the demyelinating neuropathy CMT1B.

P0 glycoprotein is a 28 kDa single pass transmembrane protein with an immunoglobulin-like fold in its extracellular domain (ECD) (for review, see Kirschner et al., 2004). It is synthesized by Schwann cells, the myelin-forming glia of peripheral nerve. P0 accounts for >50% of total protein in myelinated nerves. X-ray diffraction (XRD) analysis of myelin, adhesion of transfected cells, and crystallography all suggest that tetramers of P0ECD interact in *trans* to compact the extracellular space from wraps of Schwann cell membrane as myelin is formed (Inouye and Kirschner, 1988; D'Urso et al., 1990; Filbin et al., 1990; Shapiro et al., 1996). In fact, >100 mutations, most in the P0ECD, are associated with neuropathy, and *Mpz*-null mice lack compaction of the myelin sheath (Giese et al., 1992). However, *MPZ*-associated phenotypes vary widely, including (1) typical CMT, (2) severe congenital hypomyelination (CH) leading to death in the first decade of life, (3) tomacula-predominant neuropathy, (4) neuropathy with focally folded myelin, and (5) even CMT2-like, predominantly axonal neuropathy, sometimes associated with lancinating pains, hearing loss, and pupillary abnormalities (for review, see Wrabetz et al., 2004a; Shy, 2005). The majority of these variants differ from the mild phenotype of heterozygous *MPZ* (*Mpz*) loss of function in man or mouse (Wrabetz et al., 2004a). This suggests that most mutant P0 proteins produce gain of abnormal function.

We previously provided proof of principle that diverse gain of function alterations of *Mpz* can produce variable neuropathy phenotypes. Mice overexpressing wild-type (WT) P0 (P0OE) by >50% develop dose-dependent CH (Wrabetz et al., 2000; Yin et al., 2000). In P0OE nerves, Schwann cell membranes spiraling around axons (inner mesaxon) are arrested by adhesion and reduced space between subsequent wraps, associated with premature arrival of P0, a gain of normal function mechanism. In contrast, mice overexpressing P0 by only 50% with a myc epitope tag

Received Sept. 9, 2005; revised Jan. 17, 2006; accepted Jan. 17, 2006.

This work was supported by grants from Telethon, Italy (S.P., M.L.F., and L.W.); the National Institutes of Health (NIH) (M.L.F. and L.W.); FISM–Italian Multiple Sclerosis Society (S.P.); and the Fondazione Mariani, Italy (L.W.). D.A.K. acknowledges research funding from the NIH (National Institute of Neurological Disorders and Stroke Grant NS39650) and institutional support from Boston College. We thank Cinzia Ferri for help with Rotarod analysis and Markus Beck for help with electrophysiology; Juan J. Archelos, David Colman, and Roberto Sitia for gifts of antibodies; and Rudolf Martini for the gift of the *Mpz*-null mice.

*L.W. and M.D. contributed equally to this work.

Correspondence should be addressed to Lawrence Wrabetz, San Raffaele Scientific Institute, DIBIT, Via Olgettina 58, 20132 Milan, Italy. E-mail: l.wrabetz@hsr.it.

DOI:10.1523/JNEUROSCI.3819-05.2006

 0270-6474/06/262358-11$15.00/0

at the mature N terminus (P0myc) produced a severe demyelinating neuropathy with tomacula and uncompaction of the myelin sheath, reminiscent of two distinct groups of CMT1B mutations (Previtali et al., 2000). The intraperiod line of P0myc sheaths (where opposing P0ECDs interact in *trans* to compact myelin) was widened, suggesting a steric, dominant-negative, gain of function mechanism.

These results prompted us to investigate gain of abnormal function in authentic mouse models of CMT1B mutations. S63 (34th residue after cleavage of the signal peptide) is conserved from fish to human (Kirschner et al., 2004), and mutations of S63 in the P0ECD (see Fig. 1) determine diverse neuropathy phenotypes. Lupski and colleagues (Warner et al., 1996) proposed that P0 deleted for S63 (P0S63del is associated with CMT1B) (Kulkens et al., 1993) would be unstable, thereby producing loss of one-half of P0 function, whereas substitution of cysteine for serine [P0S63S is associated with Déjérine-Sottas syndrome (DSS)] (Hayasaka et al., 1993) might produce aggregates and a toxic gain of function in the myelin sheath. To test this hypothesis, we produced transgenic mouse models with these alleles, in a way that only gain of function can be seen. We show here that both alleles produce gain of function, but of different types, originating from diverse intracellular locations.

Materials and Methods

Transgenic mice. All experiments involving animals were performed in strict accord with experimental protocols approved by local Institutional Animal Care and Use Committees. P0 overexpressor [Tg80.4 = Tg(Mpz)24Mes] and *Mpz*-null mice have been described previously (Giese et al., 1992; Wrabetz et al., 2000) and were maintained on the FVB/N (Taconic, Germantown, NY, or Charles River, Calco, Italy) genetic background. Transgene monomers for P0S63del and P0S63C mice were engineered by introducing the appropriate mutation (Fig. 1*B*) into exon 2 of mP0TOT by PCR-based site directed mutagenesis (Feltri et al., 1999; Wrabetz et al., 2000). Mutations were confirmed by sequence analysis. mP0TOT contains the complete *Mpz* with 6 kb of promoter, all exons and introns, and the natural polyadenylation site and a polymorphic *Bgl*II site in exon 3 (amino acid sequence conserved) that is absent from the endogenous FVB/N *Mpz* alleles. Transgenic mice were produced by pronuclear injection of FVB embryos, and five and three independent lines were established for Tg129 (S63del) and Tg130 (S63C), respectively. Genotype analysis (Southern blot and PCR) was performed as described previously (Wrabetz et al., 2000), revealing copy numbers ranging from 1 to 12 for Tg129 and from 4 to 13 for Tg130 (data not shown). The genetic designations of the lines that have been maintained from this study are: line 129.1, Tg(MpzS63del)30Mes; line 129.4, Tg(MpzS63del)31Mes; line 130.2, Tg(MpzS63C)32Mes; and line 130.3, Tg(MpzS63C)33Mes.

Tg129.4 or 130.3 and *Mpz* heterozygous-null animals were crossed to generate breeders for the rescue experiments (see Fig. 3). Southern blot analysis (Wrabetz et al., 2000) distinguished genotypes of offspring (data not shown).

Tunicamycin (50 μg/ml in 150 mM dextrose/1 μg/g body weight) was injected intraperitoneally, and mice were killed by CO_2 inhalation 48 or 72 h later to harvest liver and sciatic nerve for preparation of total RNA.

Behavioral analysis. Posture and gait were observed as described previously (Feltri et al., 2002; Bolino et al., 2004). Tremor was estimated visually on a + to ++++ scale. Motor ability was assessed using the accelerating Rotarod (Ugo Basile, Comerio, Italy). Groups of 4-month-old transgenic and control littermates were tested in two sessions of three trials each per day (6 h rest between the two daily sessions) for 3 consecutive days. During the test, the rod accelerated from 4 to 40 rotations per minute, and the time that the animal remained on the rod (maximum, 900 s) was measured.

Electrophysiologic analysis. Electrophysiologic analysis was performed as described previously (Zielasek et al., 1996). In brief, under light anesthesia, peripheral nerves were stimulated by short electric pulses, and the ensuing compound muscle action potentials (CMAPs) were recorded with a differential amplifier (92b; Medelec, Woking, UK). For facial nerve motor conduction studies, stimulating steel needle electrodes were placed subcutaneously in the left outer ear canal (active) and behind the ear (inactive). Recording needle electrodes were placed in the whisker muscles. For sciatic nerve motor conduction studies, stimulating electrodes were placed in the left sciatic notch and 2 cm laterally (proximal), or subcutaneously along the tibial nerve just above the ankle (distal). Recording electrodes were placed in the dorsal skin of the foot to record CMAPs from the small muscles of the foot. Motor conduction velocities, CMAP amplitudes and latencies, and F-wave latencies were determined as described previously. For sciatic nerve afferent conduction velocity studies, mixed afferent sciatic nerve potentials were recorded at the sciatic notch after stimulation at the ankle. Mixed afferent sciatic nerve potential denotes compound nerve action potentials that include orthodromically stimulated sensory fibers and antidromically stimulated motor fibers.

Reverse-transcription PCR and quantitative Taqman analysis. Sciatic nerves or livers were dissected from transgenic and nontransgenic littermates at the indicated ages and frozen in liquid nitrogen. Total RNA was prepared with Trizol (Roche Diagnostics, Mannheim, Germany), and reverse transcription-PCR (RT-PCR) was performed as described previously (Feltri et al., 1999). To measure the amount of transgenic relative to endogenous *Mpz*, RT-PCR products were digested with *Dpn*II, which distinguishes wild-type FVB/N from transgenic BALB/c *Mpz* cDNA (BALB/c *Mpz* contains the *Dpn*II polymorphism) (Wrabetz et al., 2000). A representative autoradiogram from repeat experiments on three animals for each genotype is shown in Figure 1. For RT-PCR analysis of X-box binding protein 1 (XBP1) splicing, the same volume of RT products was used to amplify glyceraldehyde-3-phosphate dehydrogenase (GAPDH) [forward (F), 5′-GTATGACTCTACCCACGG and reverse (R), 5′-GTTCAGCTCTGGGATGAC] or XBP1 (forward, 5′-CCTTGTGGTTGAGAACCAGG and reverse, 5′-GGCTTGGTGTATACATGGTC). A representative image from repeat experiments on five independent groups of mice is shown in Figure 7. Semiquantitative RT-PCR for BiP (binding Ig protein) and CHOP (CAATT enhancer-binding protein homologous protein) mRNA was performed with radiolabeling as described previously (Feltri et al., 1999). The input RT for BiP or CHOP was normalized by previous GAPDH amplification. Primers were the following: BiPF, CCCAGCGACAAGCAAC; BiPR, CTTTCTGGACAGGCTTC; CHOPF, CCCTGCCTTTCACCTTG; CHOPR, CGTCCGTGTGGTCTCC.

Quantitative RT-PCR was performed as per manufacturer's instructions (Taqman; Applied Biosystems, Monza, Italy) on an ABI PRISM 7700 sequence detection system (Applied Biosystems), using total RNA prepared from P28 sciatic nerves as above. Four hundred nanograms (BiP) or 4 μg (CHOP) of RNA were reverse transcribed in 1 mM dNTPs, 2.5 ng/μl random hexamers, 40 U RNasin (Promega, Madison, WI), and 20 U AMV reverse transcriptase (BiP; Promega) or SuperScript II RNase H$^-$ reverse transcriptase (CHOP; Invitrogen, San Giuliano Milanese, Italy). Samples were incubated for 10 min at room temperature and then for 1 h at 42°C. Target BiP and CHOP mRNAs and reference 18S rRNA were measured in separate tubes using the Assay on Demand Mm00517691_m1, Mm00492097_m1, and Hs99999901_s1 (Applied Biosystems), respectively. Normalization was performed with the relative standard curve method using total RNA from littermate wild-type sciatic nerves as the reference.

Western blot analysis. Sciatic nerves were dissected from transgenic and nontransgenic littermates, snap-frozen in liquid nitrogen, and analyzed as described previously (Wrabetz et al., 2000). The primary antibodies included mouse monoclonal anti-P0 (P07; Juan Archelos, University of Graz, Graz, Austria) and anti-β-tubulin (Sigma, St. Louis, MO). Anti-mouse peroxidase-conjugated secondary antibody (Sigma) was visualized using the ECL method and autoradiography (Amersham Biosciences, Essex, UK). The intensity of bands was quantified by densitometry, and the ratio of intensities for P0 and β-tubulin was determined. For deglycosylation experiments with peptide *N*-glycosidase F (PNGaseF) and endoglycosidase H (EndoH), homogenates were digested per manufacturer's instructions (New England Biolabs, Beverly, MA) and visualized as described above.

Morphological analysis. Semithin section and EM analyses of sciatic and digital nerves of transgenic and control littermates were performed as described previously (Quattrini et al., 1996; Frei et al., 1999). Usually, three to five animals were analyzed at each time point for each transgenic line. For periodicity analysis, electron micrographs at 20,000× magnification of multiple mutant or wild-type sciatic nerves were photographed in the same session to avoid changes in equilibration of the electron beam.

Immunohistochemistry analysis. Postnatal day 28 sciatic nerves from transgenic and control mice were dissected, cryoprotected in 20% sucrose, embedded in OCT (Miles, Elkhart, IN), and snap frozen in liquid nitrogen. Cryosections, 6–8 μm thick, were fixed in 4% paraformaldehyde for 4 min at room temperature, followed by immersion in cold acetone for 10 s and two rinses in PBS. Specimens were blocked in 0.1% Triton X-100, 1% BSA, and 15% normal goat serum in PBS for 20 min at room temperature. After 15 min incubation with polyclonal anti-P0 antibody (diluted 1:1000; D. Colman, Montreal Neurological Institute, Montreal, Quebec, Canada), sections were rinsed in PBS and incubated for 1 h with monoclonal anti-KDEL antibody [diluted 1:200; antibodies to this signal recognize primarily BiP chaperone and two other proteins, located in the endoplasmic reticulum (ER) and *cis*-face of the Golgi apparatus; Stressgen, Victoria, British Columbia, Canada], rinsed in PBS, and incubated with FITC- and rhodamine- (tetramethylrhodamine isothiocyanate) conjugated secondary antibodies (The Jackson Laboratory, Baltimore, MD), mounted with Vectashield (Vector Laboratories, Burlingame, CA), and examined on a fluorescence microscope (AX-70; Olympus, Melville, NY). Image analysis was performed with Adobe Photoshop CS (Adobe Systems, San Jose, CA).

XRD analysis. Sciatic nerves were dissected, sealed in quartz capillary tubes in physiological saline (154 mM NaCl, 5 mM Tris buffer, pH 7.4), and analyzed within 30 min as described previously (Avila et al., 2005). Diffraction experiments used a fine-line source on a 3.0 kW Rigaku (The Woodlands, TX) x-ray generator operated at 40 kV by 14–22 mA and a linear, position-sensitive detector (Molecular Metrology, Northampton, MA) (Avila et al., 2005). Patterns were recorded for 10 min. Seven hours later, another pattern was recorded for 2 h to detect any swelling occurring under physiological conditions. Wild-type nerves showed no swelling under these conditions. Measurement of the positions of the reflections in the myelin diffraction pattern revealed the periodicity of myelin, and quantitation of the intensities above background permitted calculation of membrane profiles. From the membrane profiles, we measured the widths of the extracellular and cytoplasmic appositions and the thickness (distance between the lipid polar head groups) of the membrane bilayer. These structural parameters are determined as the distances between the middles of the headgroup layers across the intermembrane (extracellular and cytoplasmic) spaces and within a single bilayer. The disorder in the stacking of membranes in multilamellar myelin was determined by plotting the integral widths w^2 as a function of h^4, where the intercept on the ordinate axis is inversely related to the number of repeating units N (the coherent domain size), and the slope is proportional to the fluctuation in period Δ (lattice or stacking disorder) (Inouye et al., 1989). The relative amount of multilamellar myelin among the samples was determined by measuring the total integrated intensity (M) above background (B; after excluding the small angle region of the pattern around the beam stop as well as the wide-angle region of the pattern) for samples having equivalent exposure times. We have shown previously that a scatter plot of the fraction of total scattered integrated intensity that

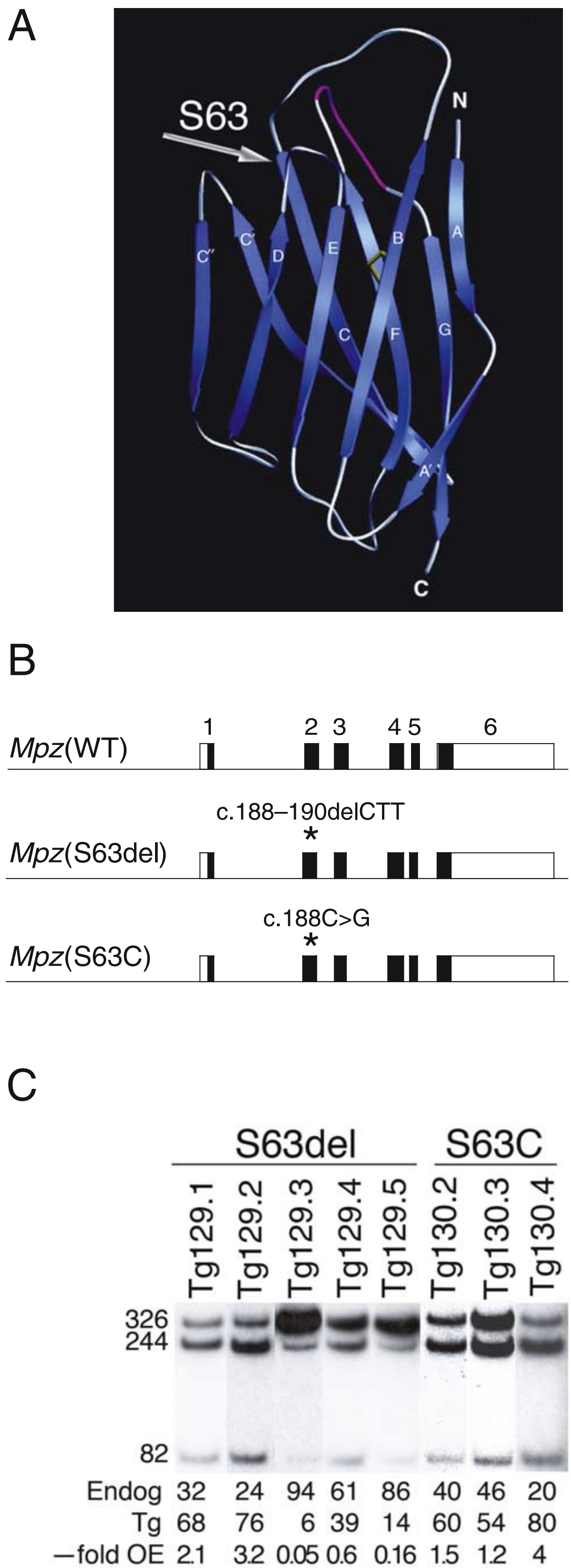

Figure 1. Characterization of S63 transgenic mice. ***A***, Ribbon diagram of P0 ECD demonstrates the location of S63 at the beginning of β-strand C [arrow; adapted from Shapiro et al. (1996) with permission of Elsevier]. ***B***, Diagram of the six exons of wild-type *Mpz*, TgS63del, and S63C with nucleotide alterations indicated by asterisks. ***C***, Semiquantitative RT-PCR analysis of transgene expression. RT product was amplified by a primer pair that recognized identically either endogenous *Mpz* or TgS63 cDNAs. *Dpn*II digestion distinguished endogenous (Endog; 326 nt band) from TgS63 (244 and 82 nt bands). Overexpression (—fold OE) is the ratio Tg/Endog signals.

 J. Neurosci., February 22, 2006 • 26(8):2358–2368

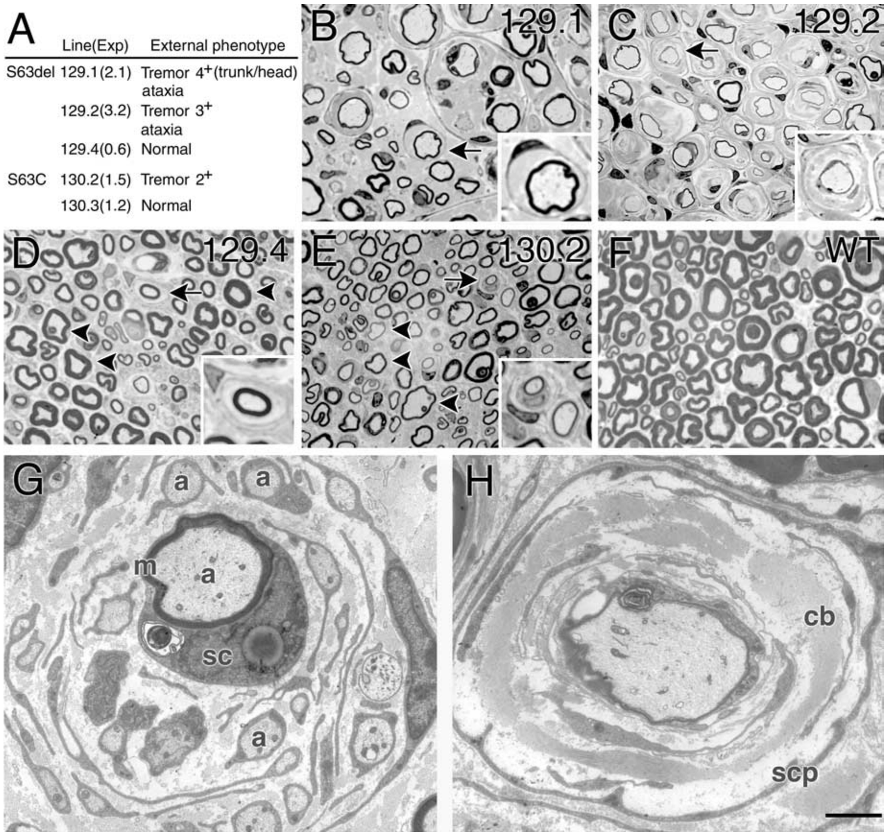

Figure 2. Phenotypes of S63 mutant mice in a wild-type (*Mpz*+/+) background. ***A***, Table describing the features of S63 phenotypes. Exp, Expression from Figure 1. ***B–H***, Morphological analysis of 1.5- to 2-year-old S63 mutant mice reveals myelin alterations. S63del sciatic nerves contain florid onion bulbs [indicated by arrows and magnified 2.5× in insets; lines 129.1 (***B***), 129.2 (***C***), 129.4 (***D***)] compared with WT (***F***). Ultrastructural analysis of S63del129.2 sciatic nerve (***C***) shows two types of onion bulbs, one with multiple Schwann cell processes in various relationships with multiple small axons (***G***), the other with multiple Schwann cell processes interspersed in collagen fibers, surrounding a single thinly myelinated axon (***H***). Endoplasmic reticulum and Golgi appeared normal. In contrast, S63C sciatic nerves [130.2 (***E***)] show more hypomyelination (compare arrowheads in ***E–D***) and less onion bulb formation. a, Axon; m, myelin; sc, Schwann cell; cb, collagen bundle; scp, Schwann cell process. Scale bar: (in ***H***) ***B–F***, 20 μm; ***G–H***, 3 μm.

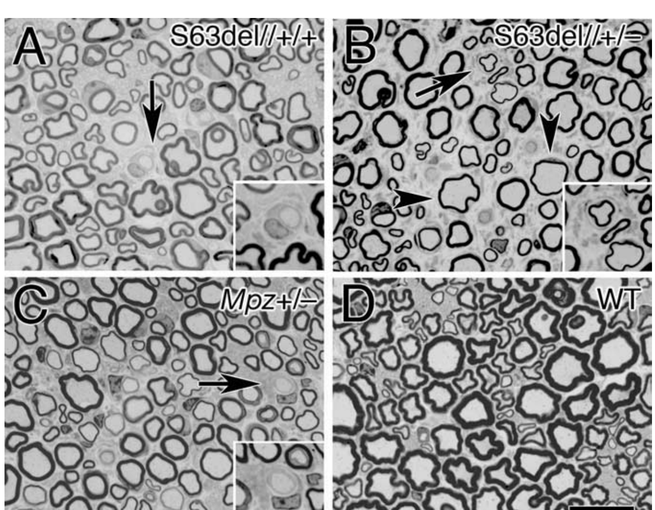

Figure 3. The S63del demyelination phenotype is not rescued by reduced *Mpz* dosage. TgS63del (***A***) was bred into the *Mpz*+/− background (S63del//+/−; ***B***) and compared with *Mpz*+/− (***C***) and WT (***D***) animals. Semithin section analysis of sciatic nerves from 16-month-old mice show that S63del//+/− nerves continue to manifest onion bulbs (arrows; magnified 2.5× in insets) and thin myelin sheaths (arrowheads) despite near normal *Mpz* dosage. The images are representative of multiple, randomly selected fields in sciatic nerve for each genotype. Scale bar: (in ***D***) 30 μm.

is attributable to myelin [*M/(M + B)*] versus myelin period (*d*) permits distinction of different dysmyelinating phenotypes (Avila et al., 2005).

Results

We showed previously that transgenes containing the wild-type *Mpz* (from 6 kb upstream to 0.5 kb downstream of coding exons) (Fig. 1) were appropriately regulated (Feltri et al., 1999; Wrabetz et al., 2000). To test whether different mutations of S63 act through gain of function, we introduced mutations in the transgene monomer that encode either deletion of S63 (P0S63del) or substitution of cysteine for serine (P0S63C) (Fig. 1) and produced transgenic mice by random insertion. Because both wild-type alleles remain in these mice, loss of function of the transgenic allele will be compensated. Only gain of function from the transgenic allele should be detected. We established multiple lines for each transgene with variable numbers of copies inserted. Expression ranged widely among lines, but several lines overexpressed transgenic mRNA at <80% of endogenous *Mpz* (Fig. 1), the window in which overexpression of wild-type *Mpz* produces barely detectable or no neuropathy (Wrabetz et al., 2000).

Both P0S63 mutants produce gain of function

Notably, both S63del and S63C lines developed evident neuromuscular disorders between 4 and 8 weeks of age, characterized by tremor, ataxia, weakness, and muscle atrophy in the hindlimbs (Fig. 2). Lines with higher expression developed more obvious defects. Analysis of semithin sections of sciatic nerve stained with toluidine blue demonstrated demyelinating neuropathy. In both S63del and S63C nerves, we noted hypomyelination with occasional nude axons. Strikingly, onion bulbs, the hallmark of hereditary demyelinating neuropathies, which signify myelin destruction followed by attempts to remyelinate, were present at 6 months of age and increased in number afterward. After 1 year of age, S63del line 129.2 showed the most florid onion bulbs ever reported in transgenic mice. Even S63del line 129.4, with only 60% overexpression, developed onion bulbs. Analysis of 6-month-old S63del line 129.4 mice revealed demyelination and occasional onion bulbs in both ventral (motor) and dorsal (sensory) roots (data not shown), as well as sciatic nerve (Fig. 2*D*). Onion bulbs were never detected at any age or dosage in mice overexpressing wild-type P0 (Wrabetz et al., 2000). In addition, such florid onion bulbs were not noted in P0 heterozygous null mice of similar ages (Fig. 3) (Martini et al., 1995). S63C mice manifested more hypomyelination and less onion bulbs than S63del at all dosages. Thus, both P0S63del and P0S63C produce dose-dependent, gain of function demyelination phenotypes that differ from the congenital hypomyelination seen with P0 overexpression.

To directly examine the role of *Mpz* overexpression in TgS63 phenotypes, we crossed them into P0-deficient backgrounds to reduce total *Mpz* expression to near wild-type levels (100%). The S63del line Tg129.4 was crossed into *Mpz*+/− background (160% reduced to 110% total *Mpz* expression), and the S63C line Tg130.3 was crossed into the *Mpz*-null background (220% reduced to 120% total *Mpz* expression), and sciatic nerves from animals 12–18 months of age were examined by semithin section analysis. Although the comparable P0OE mouse crossed into the *Mpz*−/− background (180% reduced to 80% total *Mpz* expression) showed almost complete rescue of hypomyelination phenotype (Wrabetz et al., 2000), neither TgS63 phenotype was ameliorated by reducing P0 dosage. Onion bulbs remained in both cases (Fig. 3*B* and data not shown). Thus, both P0S63del and P0S63C produce gain of abnormal function independent of P0 overexpression.

S63del//P0+/− mice model CMT1B

To validate the S63del//+/− mice as a model of CMT1B (both the mouse and human carry one mutant allele and one WT allele), we performed behavioral, electrophysiological, and morphological analysis. Although gait analysis of adult S63del//+/− did not reveal an overt disorder, mutant mice were able to remain for only half as long on an accelerating Rotarod compared with WT mice (Fig. 4). Consistent with this neuromuscular impairment, electrophysiological analysis in sciatic nerve revealed markedly slowed nerve conduction and prolonged F-wave latencies, suggesting myelin abnormalities with important functional consequences (Table 1). The trace of the CMAP did not demonstrate major polyphasia and temporal dispersion was mild (Fig. 4), suggesting uniform changes throughout the myelin, as reported for human CMT1 neuropathies (Kaku et al., 1993). CMAP amplitudes in both facial and sciatic nerves showed a trend toward reduction, compatible with axonal loss.

Morphological analysis showed onion bulbs and thin myelin sheaths, all more pronounced distally in digital nerves. We also noted reduced numbers of myelinated fibers (Fig. 4) and occasional axonal degeneration in digital nerves (data not shown), consistent with reduced CMAP amplitudes. These changes progressed with age (Fig. 4). The S63del//+/− mice were more affected than control *Mpz*+/− mice. Thus, these mice model all of the features of progressive, length-dependent CMT1B neuropathy. In addition, the lack of rescue with reduced *Mpz* gene dosage, together with a more severe phenotype than *Mpz*+/− mice, emphasizes that P0S63del produces an additional gain of abnormal function.

S63 mutants traffic to diverse intracellular locations

In order for P0S63del and P0S63C to produce gain of function, they must be synthesized. Therefore, we measured protein levels by Western blot analysis. To detect only mutant protein, we crossed either S63 mutant onto the *Mpz*-null background. We detected S63C at the same relative molecular weight as wild type, but at about one-half of wild-type levels (Fig. 5), consistent with reduced myelination seen in semithin sections (Fig. 2). Surprisingly, S63del demonstrated an M_r 4 kDa smaller than WT or S63C proteins. This alteration was not specific to the P0 null background, because a similar band could be detected in wild-type or heterozygous null backgrounds, and even in nontrangenic mice. This suggested that a post-translational modification that normally occurs in P0WT was altered for P0S63del. In addition, the amount of P0S63del was more clearly reduced, to 1% of wild type. To explore whether this was transcriptionally mediated, we measured total *Mpz* (endogenous and transgenic)

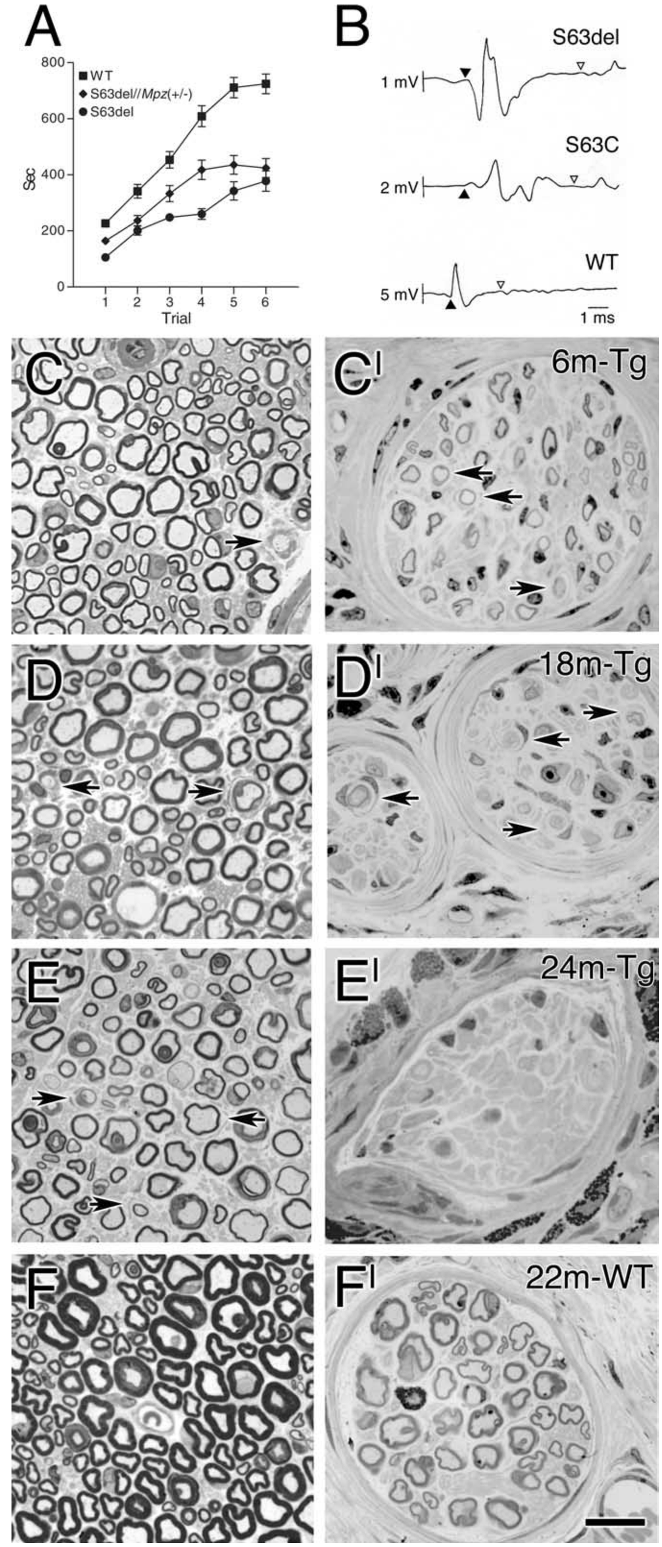

Figure 4. S63del//*Mpz*+/− mice provide a good model of human CMT1B neuropathy. ***A***, Rotarod analysis shows that S63del//+/− remain on the accelerating cylinder about one-half the time of wild type. Error bars represent SEM; $n = 10$. ***B***, CMAPs were recorded from the small foot muscles after supramaximal proximal sciatic nerve stimulation. Shown are redrawn original recordings from 1-year-old mice. The filled triangles indicate the onset of the M-response; the open triangles indicate the onset of the F-wave. Note the different amplitude scales. Semithin section analysis of mutant (***C/C′–E/E′***) and wild-type (***F***, ***F′***) sciatic (***C–F***) or digital (***C′–F′***) nerves reveals onion bulbs (arrows) and hypomyelination, which are more evident distally and progress with age. m, Month. Scale bar: (in ***F′***) 25 μm.

Table 1. Electrophysiological analysis of 12-month-old S63del//*Mpz*+/− mice

	Mot CV (m/s)	Mix. aff. NCV (m/s)	F-wave lat (ms)	CMAP amp (mV)	CMAP lat (ms)
Facial nerve					
S63del//*Mpz*+/−				7.9 ± 1.2[a]	1.25 ± 0.12
WT				10.6 ± 1.2	1.08 ± 0.04
Sciatic nerve					
S63del//*Mpz*+/−					
Prox				7.3 ± 2.0	
Dist	24 ± 1.2*	38 ± 5.2*	8.6 ± 0.2*	8.2 ± 1.7*	1.27 ± 0.12*
WT					
Prox				10.6 ± 1.4	
Dist	43 ± 4.6	60 ± 4.6	5.1 ± 0.2	14.1 ± 1.4	0.92 ± 0.05

[a]Mean ± SEM; $n = 3$ for all genotypes.

Mot CV, Motor nerve conduction velocity; Mix. aff. NCV, mixed afferent NCV; amp, amplitude; lat, latency; Prox, proximal; Dist, distal. *$p < 0.05$ relative to WT by *t* test.

mRNA in wild-type and homozygous *Mpz*-null backgrounds and compared the result to the protein levels as measured by Western analysis. Control heterozygous *Mpz*-null nerves contained approximately one-half of wild-type *Mpz* mRNA and P0 as expected. S63delWT nerves contained 178% *Mpz* mRNA compared with WT when normalized by GAPDH mRNA, as predicted by RT-PCR analysis relative to endogenous *Mpz* in Figure 1 (60% overexpression) and 63% P0 protein compared with WT when normalized to tubulin, probably because of reduced bulk myelin (Fig. 2). In contrast, S63del//*Mpz*-null nerves contained 43% *Mpz* mRNA, but only 1% P0. In sum, these data suggest that the post-translational modification of P0S63del is altered and that P0S63del may be unstable.

Diverse gain of function phenotypes suggest diverse pathomechanisms. The first step to determine these mechanisms is to locate the mutant proteins intracellularly. Therefore, we immunostained for P0 and KDEL in Schwann cells in nerves from S63 mutant//*Mpz*-null mice. Proteins that contain the KDEL peptide are retained/recycled to the ER (Munro and Pelham, 1987). Figure 6 shows that P0S63C, like wild-type P0, arrived to the myelin sheath, whereas P0S63del colocalized with KDEL, suggesting it is retained for the most part in the ER.

We explored the alteration in post-translation modification of P0S63del to more precisely locate where the mutant protein was blocked in trafficking. One obvious explanation would be altered glycosylation. P0 is normally glycosylated at N93 (N122 in the nomenclature used for the mutations) of the mature ECD in the Schwann cell ER (D'Urso et al., 1990). In the pre-Golgi and *cis*-Golgi spaces, N-linked glycoproteins contain immature, high-mannose oligosaccharides that are sensitive to digestion with EndoH. After arrival to the medial-Golgi stacks, oligosaccharides are converted to mature, complex type and become EndoH resistant. Normal myelin contains both EndoH-resistant and EndoH-sensitive P0 (Brunden, 1992). PNGaseF cleaves N-linked oligosaccharides independently of their maturation. Western analysis of S63mutant//*Mpz*-null nerve lysates after EndoH or PNGaseF digestion (Fig. 5*D*) showed that P0S63C is glycosylated like WT, consistent with arrival to myelin, whereas the majority of P0S63del is not glycosylated, consistent with ER retention.

Packing defect in S63C nerves

These data suggest that P0S63C produces an abnormal effect in the sheath, whereas P0S63del does not. To evaluate a possible packing defect that could produce myelin instability, we characterized by EM the ultrastructure of S63mutant//*Mpz*-null sheaths, where again only the mutant protein is present (Fig. 6). Whereas S63del//−/− resembled an *Mpz*-null sheath, consistent with little or no arrival of mutant protein to the sheath, S63C//−/− had compacted sheaths with a regular periodic structure. However, the periodicity was expanded by 21% (Fig. 6*K* vs *J*), and most of this seemed to derive from the intraperiod line, corresponding to the extracellular apposition that contains the P0ECD.

To examine whether P0S63C produces abnormal packing even in the presence of wild-type P0, we analyzed periodicity by XRD (Kirschner and Ganser, 1980; Avila et al., 2005). Ultrastructural analysis of S63C//+/+ and S63C//+/− nerves had revealed irregular areas of "splitting" of the intraperiod line, but only in a sector of sheaths (<25% of volume), such that we could not eliminate fixation artifacts (data not shown). However, XRD analysis of myelin period is more sensitive than EM and provides quantitative structural information on a large volume of internodal myelin in a nerve segment, not just a thin section like EM. Therefore, we performed XRD analysis on freshly dissected nerves from S63C//−/−, S63C//+/−, or S63C//+/+ mice. S63C//−/− myelin showed a periodicity of 210.7Å, increased 20% from WT myelin at 175Å, agreeing very well with the 21% increase detected by EM (Table 2). Analysis of the membrane profile revealed that the majority of this increase derived from the extracellular space (Table 2, ext, corresponding to the intraperiod line in EM). Neither S63C//+/− nor S63C//+/+ myelin showed altered period or intermembrane distances in the initial recording from the freshly dissected nerves. However, in S63C//+/− myelin, a swollen phase with a period of 204.7Å was detected as a shoulder on the third order reflection (data not shown). From an initial 10% of total internodal myelin, the swollen phase increased to ~40% of the total by 7 h. No swollen phase was ever detected in WT myelin. Although S63C//+/+ myelin manifested only a minor swollen phase at 7 h, analysis of linewidths of the diffracted reflections from the initial recordings (see Materials and Methods) (Avila et al., 2005) showed that both S63C//+/+ and S63C//+/− myelin contained disordered packing of membranes (Table 2, Δ). Finally, total myelin diffraction (Table 2, $M/M + B$) for both S63C//+/− and S63C//+/+ was reduced by about one-half, consistent with the idea that S63C produces hypomyelination in addition to demyelination (Fig. 2). Thus, P0S63C produces a gain of abnormal function in the myelin sheath and even in the presence of wild-type P0, consistent with a dominant-negative effect.

Unfolded protein response in S63del nerves

One possible explanation for ER retention and lack of glycosylation of P0S63del could be that it is not properly folded. As a consequence, cells typically mount an unfolded protein response (UPR) (Harding et al., 2002; Rutkowski and Kaufman, 2004), an ER stress response that activates chaperone transcription, such as BiP, attenuates protein translation, and stimulates protein degradation to reduce the load of improperly folded protein. In the case of excessive protein accumulation, the response becomes maladaptive, activating cell suicide. One important transcription factor that mediates the latter is CHOP.

Therefore, we measured BiP and CHOP message and protein levels in sciatic nerves from S63mutant nerves (Fig. 7). In fact, there was a UPR in S63del, but not in S63C or P0OE, nerves. Both

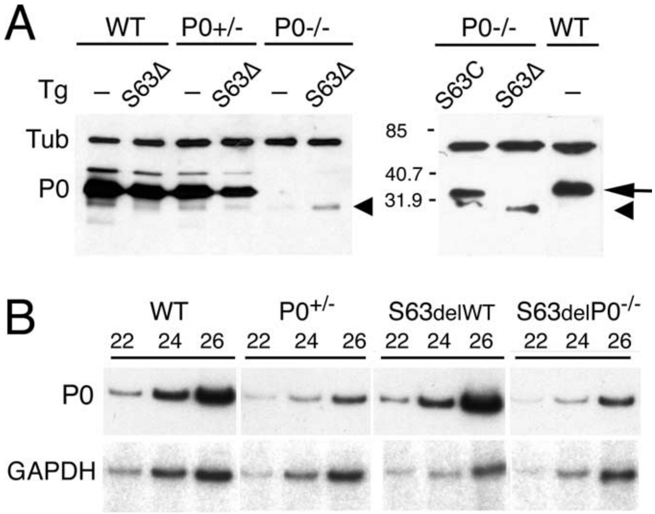

C

	mRNA	protein
P0+/-	0.74	0.49
S63delWT	1.78	0.63
S63delP0-/-	0.43	0.01

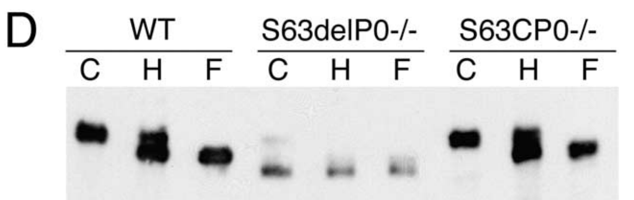

Figure 5. Biochemical and expression analysis of P0S63 mutants shows that P0S63del has altered post-translational modification and markedly reduced steady-state protein levels. ***A***, Western analysis for P0S63 mutant proteins in WT, *Mpz*+/− (P0+/−), or *Mpz*-null (P0−/−) backgrounds. Note that P0S63del migrates faster than P0WT (arrow), at a size similar to a minor band seen in all lanes (arrowhead). Tubulin (Tub) detection confirmed equal loading of protein. The numbers indicate relative molecular weights. ***B***, Semiquantitative RT-PCR analysis for P0 mRNA (P0) relative to GAPDH in sciatic nerves from *Mpz*+/− (P0 $^{+/-}$), S63del (S63delWT), or S63del in the *Mpz*-null background (S63delP0 $^{-/-}$) quantified in ***C*** relative to wild type defined as 1. The numbers in ***B*** refer to cycles of PCR amplification. ***D***, Western analysis for P0 on sciatic nerve lysates from WT or S63 mutants in the *Mpz*-null background (e.g., S63delP0−/−) untreated (C) or after digestion with EndoH (H) or PNGaseF (F). Untreated P0WT migrated with a relative molecular weight of 28.5 kDa. EndoH treatment of WT revealed ∼60% high-type (sensitive) and 40% complex-type (resistant) P0 glycosylation as reported previously in adult rat nerve homogenates (Brunden, 1992). PNGaseF digestion of P0WT completely removed oligosaccharide and produced migration at 24.8 kDa (D'Urso et al., 1990). Glycosylation of S63C was similar to that of WT. In contrast, most P0S63del was insensitive to both EndoH and PNGaseF digestion, indicating that the majority of the protein was not glycosylated at the steady state. Note that the relative molecular weight of S63del protein [S63delP0−/− (C); estimated to be 20.5 kDa] was less than that of deglycosylated P0WT [WT (F)], suggesting further post-translational differences.

BIP and CHOP mRNA were induced to levels comparable with those produced in liver 48 h (data not shown) and 72 h after tunicamycin treatment; tunicamycin blocks glycosylation in the ER and thereby produces a robust UPR. Similar changes were detected at the level of BiP and CHOP proteins in S63del nerves (data not shown). We also detected induction of another UPR mediator, alternatively spliced XBP1 (Fig. 7) (Harding et al., 2002; Rutkowski and Kaufman, 2004). Thus, retention of non-glycosylated P0S63del in the ER is associated with a significant UPR in S63del nerves.

Discussion

We describe new transgenic mouse models of two P0S63 mutations associated with CMT1B or DSS neuropathies in humans. Both S63del and S63C mice develop neuropathies that resemble the corresponding human neuropathy, and the S63del//*Mpz*+/− mice in particular represent a valid clinical model of CMT1B. Each P063 mutant acts via gain of abnormal function, but surprisingly, their pathomechanisms originate from different intracellular locations. S63C arrives to the myelin sheath where it produces a packing defect, whereas S63del is retained in the ER and induces an UPR, probably toxic to the myelin-forming Schwann cell. These data support the idea that the variability of *MPZ*-related phenotypes derive from different kinds of gain of abnormal function.

S63 mutants as models of human disease

The S63 mutant nerves resemble their respective human neuropathies. S63del sciatic nerves manifest florid onion bulbs, typical of a demyelinating neuropathy with failed remyelination like CMT1B (Kulkens et al., 1993). S63C sciatic nerves also show onion bulbs but manifest thinner myelin, which could fit with a DSS phenotype (Ouvrier et al., 1987). Most importantly, S63del//+/− mice are an excellent model of early CMT1B neuropathy in human. They show reduced neuromuscular capacity, slowed NCVs, distally accentuated demyelination and fiber loss, and progression with age. In addition, the CMAPs (Fig. 4*B*) show only minor temporal dispersion, suggesting uniform changes throughout myelin, again typical of CMT1 neuropathies (Kaku et al., 1993). Instead, significant temporal dispersion of CMAPs has been reported in other mouse models of hereditary neuropathy, for example P0OE or *Mpz*-null (Zielasek et al., 1996; Wrabetz et al., 2000), in association with gene dosage effects. One feature of CMT1B that is underrepresented histologically in S63del mice is axonal changes, reinforcing the idea that mouse lifespan, or nerve length, is too short to reveal the progressive, length-dependent fiber loss typical in human hereditary neuropathy (Frei et al., 1999; Wrabetz et al., 2004b). However, motor nerve conduction studies showed some reduction of the CMAP amplitudes in the presence of only minor temporal dispersion, which indicates that axonal damage or conduction block in some motor nerve fibers had occurred.

Because of dosage, we were not able to produce a valid model of S63C with one mutant allele and one WT allele, yet independent of P0 overexpression. The resulting S63C//+/− mouse would be predicted to express 170% of normal and manifest a P0 overexpression phenotype. In fact, S63C mice manifested temporal dispersion of the CMAP in electrophysiological analysis (Fig. 4), much like P0-overexpressing mice (Wrabetz et al., 2000). Only S63C in P0-null background (predicted 110% of wild type) would have near normal dosage, but with no wild-type allele.

S63C mice (a model of DSS) do not appear to be more severely impaired than S63del (a model of CMT1B). In the lowest-dosage S63C line, we did not see an evident external phenotype, nor were NCVs slower than those of S63del//+/− (data not shown). The most likely explanation is that the distinction between CMT1B and DSS in human is blurred; CMT1B not uncommonly appears in the first decade and manifests NCVs in the range of 5–10 m/s (Shy et al., 2004; Wrabetz et al., 2004a), and some CMT1B families contain both CMT1B and DSS phenotypes. Moreover, a median phenotype is known for S63del (multiple affected patients in two unrelated families with typical early onset CMT1B) (Kulkens et al., 1993; Numakura et al., 2002) but not for S63C, in which only one sporadic case has been described (Ouvrier et al., 1987; Hayasaka et al., 1993). Alternatively, we cannot eliminate the possibility that dosage of the S63 mutants, not yet measured in humans, differs between our mice and humans. Reduced dosage of S63C in mice could ameliorate the phenotype. None the less, P0S63C produces onion bulbs, but with thinner myelin than P0S63del, indicating different mechanisms for the two mutations at the same P0 ECD residue.

Both S63 mutants produce gain of function mechanisms

Evidence from human nerves, transfected cells, and transgenic mice support the notion of gain of function resulting from *MPZ* mutations. Specific packing defects in the myelin intraperiod line have been detected in CMT1B as a result of extracellular domain mutations (e.g., R98H, R98C) (Kirschner et al., 1996), suggesting that the mutant proteins are synthesized and inserted into the myelin sheath. When cotransfected with wild-type P0, either P0 truncated in the cytoplasmic domain or P0 unable to form a disulfide bond in the extracellular domain impaired the adhesion of wild-type P0 between Chinese hamster ovary cells, suggesting a dominant-negative gain of function effect (Wong and Filbin, 1996; Zhang and Filbin, 1998). Finally, transgenic mice overexpressing wild-type P0 manifest CH because of gain of normal function (Wrabetz et al., 2000; Yin et al., 2000), whereas mice expressing P0myc develop CMT1B-like neuropathy,

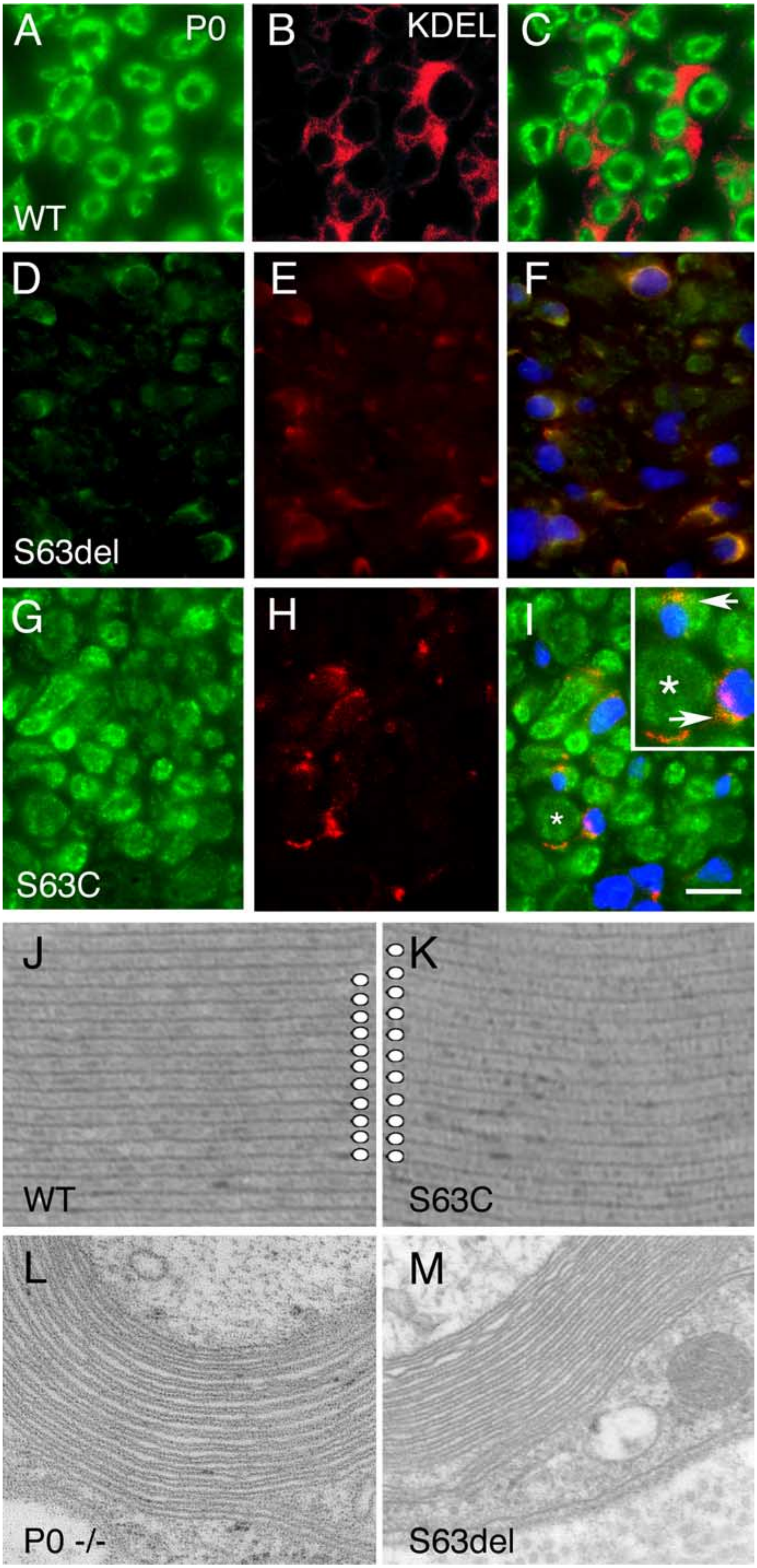

←

Figure 6. P0S63 mutant proteins arrive to diverse intracellular locations. Immunofluorescence staining for P0 (***A***, ***D***, ***G***) or KDEL (***B***, ***E***, ***H***) or overlay of the two (***C***, ***F***, ***I***) in WT (***A–C***), S63del (***D–F***), or S63C (***G***, ***H***) sciatic nerves. P0 and KDEL staining were almost mutually exclusive in wild-type nerves, with most P0 staining in circular myelin sheaths. S63C nerves were similar, except for occasional yellow overlay staining (arrows in inset; magnified 2×; asterisk in ***I*** indicates the same fiber). In contrast, almost all P0 and KDEL staining coincided in S63del nerves. Ultrastructural analysis of periodicity (***J–M***) showed that both wild-type and S63C myelin sheaths were compacted but that the periodicity (white circles indicate 11 major dense lines equal to 10 periods) was 21% larger in S63C myelin. In contrast, S63del, like *Mpz* −/− (P0 −/−) myelin, was uncompacted. Note that all S63 mutants have been bred into the *Mpz*-null background in this figure. Scale bar: (in ***I***) ***A–I***, 20 μm; ***J***, ***K***, 50 nm; ***L***, ***M***, 160 nm.

Table 2. XRD analysis of S63C myelin

	Dimensions (Å)					
Genotype	*d*	cyt	lpg	ext	Δ	*M*/(*M* + *B*)
WT	175.0 ± 0.17	31	48	47	3.7	0.347
S63C//+/+	174.3 ± 0.23	31	47	49	4.9	0.170
S63C//+/+ (7 h)	173.1 ± 0.12 (218; 6%)	32	46	48		0.152
S63C//+/−	174.9 ± 0.40	31	48	49	4.6	0.208
S63C//+/− (7 h)	173.2 ± 0.40 (204.7 ± 2.26; 41%)					
S63C//−/−	210.7 ± 0.23*	33	49	80	12.0	0.127

d, Myelin period expressed as mean ± SEM for n = 4 Bragg order reflections (values in parentheses indicate minor swollen phase and percentage of swollen arrays); cyt, the cytoplasmic separation; lpg, distance between polar headgroups; ext, the extracellular separation; Δ, lattice disorder parameter. *M*/(*M* + *B*) is the ratio of intensity in the reflections of myelin to the total intensity in the diffraction pattern (Avila et al., 2005). Initial 10 min x-ray exposures were recorded <30 min after dissection. The 7 h patterns were 2 h exposures. *$p \ll 0.001$ relative to WT by Student's *t* test.

with both tomacula and uncompaction of the myelin sheath, as a result of a dominant-negative gain of abnormal function (Previtali et al., 2000).

The S63 mutant mice then provide conclusive genetic proof of principle that gain of function is sufficient to produce varying CMT phenotypes. Structural consideration of the two mutants predicted a diverse gain of function for both S63 mutants. Deletion of S63 likely alters the polarity of the following β strand producing unfolding and ER retention. Instead, introduction of a cysteine residue at position 63 produces exposes thiols that still permit arrival to the myelin sheath but create local problems there. This is as Lupski and colleagues (Warner et al., 1996) had predicted, but the surprise is that ER retention produces gain of function, in addition to the loss function related to the absence of mutant P0 in the sheath. In keeping with gain of function is that demyelination appeared even with two normal copies of the P0 gene present. Myelin abnormalities are not caused by P0 overexpression, because we never observed onion bulbs in P0OE mice, and when we reduce total P0 dosage by breeding S63del into the heterozygous null background, the demyelinating phenotype is not rescued. Moreover, the phenotype of S63del is more severe than *Mpz* heterozygous null (+/−) mouse. For example, motor NCV is reduced by 50% in S63del//+/− and only ~30% in +/− mice [Table 2 and Martini et al. (1995); analysis performed by the same investigators (J.Z. and K.T.)]. Together with the P0OE and P0myc mice, S63mutant mice provide four models of *Mpz*-related neuropathies ranging from severe CH to tomaculous/uncompaction to demyelinating onion bulb neuropathy. These observations provide strong support for the idea that diverse human phenotypes associated with *MPZ* genetic alterations result from diverse gain of function mechanisms deriving from various intracellular locations.

The S63 mice are the first example of authentic CMT1B mutations that produce gain of function independent of P0 overexpression. In contrast, for another recently published *Mpz* missense mutation, P0I135L (Runker et al., 2004), only two transgenic lines, each with 600% P0 overexpression, were reported. Unfortunately, the developmental effects of P0 overexpression were not eliminated, especially relevant because P0I135L mice manifested predominantly hypomyelination, typical of P0 overexpression (Wrabetz et al., 2000).

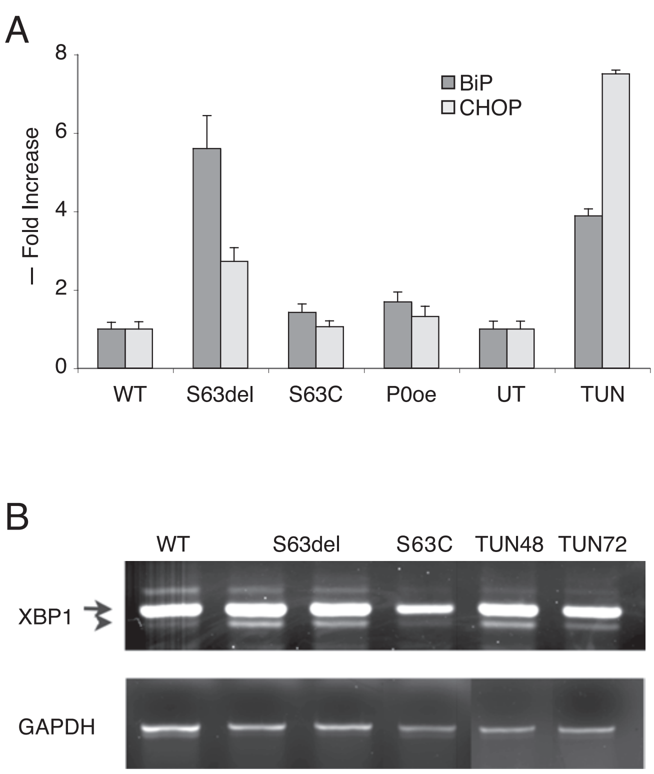

Figure 7. S63del sciatic nerves manifest a UPR. ***A***, Quantitative real-time RT-PCR analysis for BiP and CHOP mRNA levels relative to WT set arbitrarily to 1. All values (mean ± SEM for $n = 5$ mice, all in *Mpz*+/+ background) were first normalized to 18S rRNA levels. Note that BiP and CHOP levels were significantly increased in S63del compared with S63C, P0OE, or WT ($p < 0.01$ by Student's *t* test). Liver dissected from animals 72 h after intraperitoneal injection of tunicamycin (TUN) showed a comparable induction of BiP and CHOP mRNA levels. UT, Intraperitoneal saline injection. ***B***, RT-PCR analysis for induction of XBP1 splicing shows that the XBP1 splice variant (arrowhead) appears below XBP1 (arrow) in sciatic nerves from two S63del mice and from animals at 48 h (TUN48) or 72 h (TUN72) after injection of tunicamycin, but not from wild-type or S63C mice.

P0S63C introduces a packing defect in myelin

P0S63C myelin shows altered periodicity. As the proportion of P0S63C in total P0 increases, the period expands from 174 to 210Å. Not surprisingly, in S63C//−/− myelin, a 35Å increase is seen in the extracellular apposition, where the mutant extracellular domain resides. It is interesting that P0myc increased periodicity by 12%, without having produced evident onion bulbs, but rather induced tomacula formation and areas of uncompaction (Previtali et al., 2000). Thus, although both P0S63C and P0myc produce dominant-negative effects with widened extracellular apposition, only P0S63C produced instability as manifested by demyelination and onion bulb formation. This indicates that effects on myelin packing and their consequences are mutation specific. One possibility is that instability and myelin destruction occur only above a threshold of lost extracellular apposition/adhesion. It will be fascinating to correlate the onset and type of myelin pathology, and XRD measures of widened extracellular apposition and disordered packing, with XRD measures of myelin stability in freshly dissected nerves subjected to stress, such as altered pH or ionic strength (Avila et al., 2005) in these and other mutant mice. Notably, in the myelin that mimics the human situation (S63C//+/−), a swollen phase coexists with a normal phase, whereas the swollen phase is not detected in the presence of more WT P0 (S63C//+/+). This could suggest addition of WT P0 as a treatment strategy for dominant-negative effects of mutant P0 in the myelin sheath.

P0S63del elicits a UPR

Massive cellular synthesis of myelin lipids and proteins is necessary to support myelinogenesis. Not surprisingly, therefore, autophagic (lysosomal), proteasomal, and ER stress (including UPR) arms of protein quality control have been implicated in myelin disorders. For example, several recently identified CMT genes [*NDRG1*(CMT4D), *MTMR2* (CMT4B1), *MTMR13* (CMT4B2), and *LITAF* (CMT1C)] have putative Schwann cell-autonomous functions that may relate to quality control (Berger et al., 2004; Bolino et al., 2004; Wrabetz et al., 2004a). Second, lysosomal storage diseases produce leukodystrophies such as metachromatic or globoid cell leukodystrophy. Third, some mutant PMP22 proteins (CMT1A) may be retained in the ER, retrotranslocated for degradation, then aggregate and lead to inefficient proteasome function, toxic to the cell (Notterpek et al., 1999; Fortun et al., 2005). Fourth, various mutations in subunits of eukaryotic translation factor EIF2B (its substrate, EIF2α, is an important component of ER stress response), produce vanishing white matter disease (Proud, 2001). Finally, UPR activation was recently associated with central myelinopathy in mouse models of Pelizaeus Merzbacher disease, attributable to mutations of proteolipid protein, and in mice with enforced expression of interferon-γ in the CNS. Moreover, genetic modulation of the UPR altered the severity of the disease in both of these mouse models (Southwood et al., 2002; Lin et al., 2005).

Is it feasible that UPR associated with S63del ER retention could produce demyelination? One possibility is that CHOP induction activates Schwann cell apoptosis. Pelizeaus-Merzbacher myelinopathy is associated with UPR and apoptosis of oligodendrocytes (Southwood et al., 2002). However, we have not observed an obvious reduction in numbers of Schwann cells in S63del nerves or a phenotype typical of extensive Schwann cell death (Messing et al., 1992). Another possibility is that UPR could perturb stoichiometry; it broadly attenuates translation and alters transcription, and single UPR mediators alter the balance of protein and lipid synthesis (Sriburi et al., 2004). Altered dosage of either single myelin proteins or lipid enzymes, or the program of myelin gene expression, is associated with myelinopathies in man or mouse (Popko et al., 1999; Nagarajan et al., 2001; Wrabetz et al., 2004b). UPR effects limited to pivotal regulators would also be sufficient to induce demyelination. Disruption of *EGR2/Krox20* blocks myelination and *EGR2* mutations are associated with CMT1 or CH (Wrabetz et al., 2004a).

These findings may have important implications for the treatment of hereditary demyelinating neuropathies. Dominant-negative effects may be ameliorated by increasing WT P0 dosage, but only 50–80% overexpression of P0 produces CH neuropathy in mice (Wrabetz et al., 2000); therapeutic dosage must be precisely regulated. Instead, general toxic mechanisms will target other proteins/functions, and some even outside of the myelin sheath (e.g., P0S63del). Here, replacement therapy with wild-type P0 protein may have no effect, and other mutation-specific strategies will need to be developed.

References

Avila RL, Inouye H, Baek RC, Yin X, Trapp BD, Feltri ML, Wrabetz L, Kirschner DA (2005) Myelin membrane packing and stability in transgenic mouse models of dysmyelinating diseases. J Neuropathol Exp Neurol 64:976–990.

Berger P, Sirkowski EE, Scherer SS, Suter U (2004) Expression analysis of the N-Myc downstream-regulated gene 1 indicates that myelinating Schwann cells are the primary disease target in hereditary motor and sensory neuropathy-Lom. Neurobiol Dis 17:290–299.

Bolino A, Bolis A, Previtali SC, Dina G, Bussini S, Dati G, Amadio S, Del Carro U, Mruk DD, Feltri ML, Cheng CY, Quattrini A, Wrabetz L (2004) Disruption of Mtmr2 produces CMT4B1-like neuropathy with myelin outfolding and impaired spermatogenesis. J Cell Biol 167:711–721.

Brunden KR (1992) Age-dependent changes in the oligosaccharide structure of the major myelin glycoprotein, P0. J Neurochem 58:1659–1666.

D'Urso D, Brophy PJ, Staugaitis SM, Gillespie CS, Frey AB, Stempak JG, Colman DR (1990) Protein zero of peripheral nerve myelin: biosynthesis, membrane insertion, and evidence for homotypic interaction. Neuron 4:449–460.

Feltri ML, D'Antonio M, Quattrini A, Numerato R, Arona M, Previtali S, Chiu SY, Messing A, Wrabetz L (1999) A novel P0 glycoprotein transgene activates expression of lacZ in myelin-forming Schwann cells. Eur J Neurosci 11:1577–1586.

Feltri ML, Graus Porta D, Previtali SC, Nodari A, Migliavacca B, Cassetti A, Littlewood-Evans A, Reichardt LF, Messing A, Quattrini A, Mueller U, Wrabetz L (2002) Conditional disruption of beta 1 integrin in Schwann cells impedes interactions with axons. J Cell Biol 156:199–209.

Filbin M, Walsh F, Trapp B, Pizzey J, Tennekoon G (1990) Role of myelin P0 protein as a homophilic adhesion molecule. Nature 344:871–872.

Fortun J, Li J, Go J, Fenstermaker A, Fletcher BS, Notterpek L (2005) Impaired proteasome activity and accumulation of ubiquitinated substrates in a hereditary neuropathy model. J Neurochem 92:1531–1541.

Frei R, Motzing S, Kinkelin I, Schachner M, Koltzenburg M, Martini R (1999) Loss of distal axons and sensory Merkel cells and features indicative of muscle denervation in hindlimbs of P0-deficient mice. J Neurosci 19:6058–6067.

Giese KP, Martini R, Lemke G, Soriano P, Schachner M (1992) Mouse P0 gene disruption leads to hypomyelination, abnormal expression of recognition molecules, and degeneration of myelin and axons. Cell 71:565–576.

Harding HP, Calfon M, Urano F, Novoa I, Ron D (2002) Transcriptional and translational control in the mammalian unfolded protein response. Annu Rev Cell Dev Biol 18:575–599.

Hayasaka K, Himoro M, Sawaishi Y, Nanao K, Takahashi T, Takada G, Nicholson G, Ouvrier R, Tachi N (1993) De novo mutation of the myelin P0 gene in Dejerine-Sottas disease (hereditary motor and sensory neuropathy type III). Nat Genet 5:266–268.

Inouye H, Kirschner DA (1988) Membrane interactions in nerve myelin. I. Determination of surface charge from effects of pH and ionic strength on period. Biophys J 53:235–245.

Inouye H, Karthigasan J, Kirschner DA (1989) Membrane structure in isolated and intact myelins. Biophys J 56:129–137.

Kaku DA, Parry GJ, Malamut R, Lupski JR, Garcia CA (1993) Uniform slowing of conduction velocities in Charcot-Marie-Tooth polyneuropathy type 1. Neurology 43:2664–2667.

Kirschner DA, Ganser AL (1980) Compact myelin exists in the absence of basic protein in the shiverer mutant mouse. Nature 283:207–210.

Kirschner DA, Szumowski K, Gabreel-Festen AAWM, Hoogendijk JE, Bolhuis PA (1996) Inherited demyelinating peripheral neuropathies: relating myelin packing abnormalities to P0 molecular defects. J Neurosci Res 46:502–508.

Kirschner DA, Wrabetz L, Feltri ML (2004) The P0 gene. In: Myelin biology and disorders (Lazzarini RA, ed), pp 523–545. San Diego: Elsevier Academic.

Kulkens T, Bolhuis PA, Wolterman RA, Kemp S, te Nijenhuis S, Valentijn LJ, Hensels GW, Jennekens FG, de Visser M, Hoogendijk JE, Bass F (1993) Deletion of the serine 34 codon from the major peripheral myelin protein P0 gene in Charcot-Marie-Tooth disease type 1B. Nat Genet 5:35–39.

Lin W, Harding HP, Ron D, Popko B (2005) Endoplasmic reticulum stress modulates the response of myelinating oligodendrocytes to the immune cytokine interferon-gamma. J Cell Biol 169:603–612.

Martini R, Zielasek J, Toyka KV, Giese KP, Schachner M (1995) Protein zero (P0)-deficient mice show myelin degeneration in peripheral nerves characteristic of inherited human neuropathies. Nat Genet 11:281–286.

Messing A, Behringer RR, Hammang JP, Palmiter RD, Brinster RL, Lemke G (1992) P0 promoter directs expression of reporter and toxin genes to Schwann cells of transgenic mice. Neuron 8:507–520.

Munro S, Pelham HR (1987) A C-terminal signal prevents secretion of luminal ER proteins. Cell 48:899–907.

Nagarajan R, Svaren J, Le N, Araki T, Watson M, Milbrandt J (2001) EGR2 mutations in inherited neuropathies dominant-negatively inhibit myelin gene expression. Neuron 30:355–368.

Notterpek L, Ryan MC, Tobler AR, Shooter EM (1999) PMP22 accumula-

tion in aggresomes: implications for CMT1A pathology. Neurobiol Dis 6:450–460.
Numakura C, Lin C, Ikegami T, Guldberg P, Hayasaka K (2002) Molecular analysis in Japanese patients with Charcot-Marie-Tooth disease: DGGE analysis for PMP22, MPZ, and Cx32/GJB1 mutations. Hum Mutat 20:392–398.
Ouvrier RA, McLeod JG, Conchin TE (1987) The hypertrophic forms of hereditary motor and sensory neuropathy. A study of hypertrophic Charcot-Marie-Tooth disease (HMSN type I) and Dejerine-Sottas disease (HMSN type III) in childhood. Brain 110:121–148.
Popko B, Dupree JL, Coetzee T, Suzuki K (1999) Genetic analysis of myelin galactolipid function. Adv Exp Med Biol 468:237–244.
Previtali SC, Quattrini A, Fasolini M, Panzeri MC, Villa A, Filbin MT, Li W, Chiu SY, Messing A, Wrabetz L, Feltri ML (2000) Epitope-tagged P(0) glycoprotein causes Charcot-Marie-Tooth-like neuropathy in transgenic mice. J Cell Biol 151:1035–1046.
Proud CG (2001) Regulation of eukaryotic initiation factor eIF2B. Prog Mol Subcell Biol 26:95–114.
Quattrini A, Previtali S, Feltri ML, Canal N, Nemni R, Wrabetz L (1996) Beta 4 integrin and other Schwann cell markers in axonal neuropathy. Glia 17:294–306.
Runker AE, Kobsar I, Fink T, Loers G, Tilling T, Putthoff P, Wessig C, Martini R, Schachner M (2004) Pathology of a mouse mutation in peripheral myelin protein P0 is characteristic of a severe and early onset form of human Charcot-Marie-Tooth type 1B disorder. J Cell Biol 165:565–573.
Rutkowski DT, Kaufman RJ (2004) A trip to the ER: coping with stress. Trends Cell Biol 14:20–28.
Shapiro L, Doyle JP, Hensley P, Colman D, Hendrickson WA (1996) Crystal structure of the extracellular domain from P0, the major structural protein of peripheral nerve myelin. Neuron 17:435–449.
Shy ME (2005) HMSN related to *MPZ* (P0) mutations. In: Peripheral neuropathy, Ed 4 (Dyck PJ, Thomas PK, eds), pp 1681–1706. Philadelphia: Saunders.
Shy ME, Jani A, Krajewski K, Grandis M, Lewis RA, Li J, Shy RR, Balsamo J, Lilien J, Garbern JY, Kamholz J (2004) Phenotypic clustering in MPZ mutations. Brain 127:371–384.
Southwood CM, Garbern J, Jiang W, Gow A (2002) The unfolded protein response modulates disease severity in Pelizaeus-Merzbacher disease. Neuron 36:585–596.
Sriburi R, Jackowski S, Mori K, Brewer JW (2004) XBP1: a link between the unfolded protein response, lipid biosynthesis, and biogenesis of the endoplasmic reticulum. J Cell Biol 167:35–41.
Suter U, Scherer SS (2003) Disease mechanisms in inherited neuropathies. Nat Rev Neurosci 4:714–726.
Warner LE, Hilz MJ, Appel ST, Killian JM, Kolodny EH, Karpati G, Carpenter S, Watters GV, Wheeler C, Witt D, Bodell A, Nelis E, Broeckhoven CV, Lupski JR (1996) Clinical phenotypes of different MPZ (P0) mutations may include Charcot-Marie-Tooth type 1b, Dejerine-Sottas, and congenital hypomyelination. Neuron 17:451–460.
Wong MH, Filbin MT (1996) Dominant-negative effect on adhesion by myelin P0 protein truncated in its cytoplasmic domain. J Cell Biol 134:1531–1541.
Wrabetz L, Feltri M, Quattrini A, Inperiale D, Previtali S, D'Antonio M, Martini R, Yin X, Trapp B, Zhou L, Chiu S-Y, Messing A (2000) P0 overexpression causes congenital hypomyelination of peripheral nerve. J Cell Biol 148:1021–1033.
Wrabetz L, Feltri ML, Kleopa KA, Scherer SS (2004a) Inherited neuropathies: clinical, genetic and biological features. In: Myelin biology and disorders (Lazzarini RA, ed), pp 905–951. San Diego: Elsevier Academic.
Wrabetz L, Feltri ML, Suter U (2004b) Models of Charcot-Marie-Tooth disease. In: Myelin biology and disorders (Lazzarini RA, ed), pp 1143–1168. San Diego: Elsevier Academic.
Yin A, Kidd G, Wrabetz L, Feltri M, Messing A, Trapp B (2000) Schwann cell myelination requires timely and precise targeting of P0 protein. J Cell Biol 148:1009–1020.
Zhang K, Filbin MT (1998) Myelin P0 protein mutated at Cys21 has a dominant-negative effect on adhesion of wild type P0. J Neurosci Res 53:1–6.
Zielasek J, Martini R, Toyka KV (1996) Functional abnormalities in P0-deficient mice resemble human hereditary neuropathies linked to P0 gene mutations. Muscle Nerve 19:946–952.